HiPR+: A Protocol for Centimeter 3D Localization based on UWB

Daniel Neuhold
University of Klagenfurt
Klagenfurt, Austria
daniel.neuhold@aau.at

Aymen Fakhreddine*
Technology Innovation Institute
Abu Dhabi, United Arab Emirates
aymen.fakhreddine@tii.ae

Christian Bettstetter
University of Klagenfurt
Klagenfurt, Austria
christian.bettstetter@aau.at

ABSTRACT

HiPR+ is an approach for centimeter-accurate indoor localization. It combines distance estimation between ultra-wideband (UWB) transceivers and location estimation using an extended Kalman filter (EKF). The performance is tested with experiments on hardware platforms from Decawave. The distance estimation of HiPR+ achieves an order of magnitude better precision and a multiple improvement in accuracy compared to the company's native solution while it only takes only a fraction the time needed for range computation. We evaluate the 3D localization capabilities with two least-squares approaches and an EKF. A median accuracy below one centimeter can be attained using the proposed ranging error compensations in combination with the EKF-based positioning.

CCS CONCEPTS

• **Networks** → **Location based services**; • **Hardware** → *Sensor devices and platforms*; • **Computer systems organization** → Embedded software.

KEYWORDS

UWB; Ranging; 3D Localization; Time-of-Flight

ACM Reference Format:

Daniel Neuhold, Aymen Fakhreddine, and Christian Bettstetter. 2022. HiPR+: A Protocol for Centimeter 3D Localization based on UWB. In *Proceedings of the International Conference on Modeling Analysis and Simulation of Wireless and Mobile Systems (MSWiM '22), October 24–28, 2022, Montreal, QC, Canada.* ACM, New York, NY, USA, 8 pages. https://doi.org/10.1145/3551659.3559043

1 INTRODUCTION

There is an increasing demand for precise localization for applications in logistics, robotics, Internet-of-Things (IoT), and other domains. Various techniques and technologies are used that differ in their accuracy, precision, delay, complexity, cost, and efforts in terms of configuration [1, 15, 16]. For example, motion capturing provides highly accurate position estimation in the order of millimeters. These systems, however, involve significant efforts for installation and calibration and require a constant line of sight to the object being tracked. In that sense, motion capturing is too expensive and inflexible for some applications. A more affordable approach is the use of beacons from common radio systems, like Wi-Fi and Bluetooth, but their disadvantage is limited precision and low accuracy in the range of several meters. A viable alternative for some applications is ultra-wideband (UWB) radio technology, which uses a bandwidth several hundred times greater than Wi-Fi and Bluetooth.

Our work uses UWB transceivers for a localization approach that we call HiPR+. It can provide centimeter-level accuracy with latency below 10 ms and low configuration overhead. HiPR+ has two components: First, it uses the distance estimation (ranging) approach HiPR [23] but extends it with additional features. These improvements include: a hardware-independent software solution that performs hardware calibration to optimize the accuracy of distance estimations, runs a protocol that allows devices to join and leave in real time, operates a load balancing algorithm, and allows an increased time resolution of up to 100 measurements per second. Second, to obtain an overall localization solution, the ranging part is combined with existing solutions for the task of position estimation from estimated distances to fixed anchor points. Here, we compare three techniques: Two least square approaches and an extended Kalman filter that run on top of the ranging technique. The performance is assessed for static and mobile devices in an office environment using two commercially available UWB platforms from Decawave (now part of Qorvo). The main result is that the improved ranging in combination with the extended Kalman filter can achieve a 3D accuracy below one centimeter in our scenario.

The paper is organized as follows: Section 2 describes the setup, including hardware, network, and testbed. Section 3 introduces and assesses the ranging technique. Section 4 describes the localization techniques and compares their use by experiments. Section 5 covers related work. Section 6 concludes.

*Part of this work was carried out when Aymen Fakhreddine was affiliated with the University of Klagenfurt, Austria

MSWiM '22, October 24–28, 2022, Montreal, QC, Canada

ACM ISBN 978-1-4503-9479-6/22/10.
https://doi.org/10.1145/3551659.3559043

2 SETUP

We operate a network of UWB devices to facilitate distance measurements between them and to estimate their positions. A device takes one of two roles: it acts either as a *tag* or *access point (AP)*. A tag can be mobile and has an unknown location. An AP is static and has a know location. The APs act as anchors. A tag performs distance measurements to multiple APs and estimates its own position from these distance estimates using multilateration.

2.1 Hardware Platforms

As UWB devices we employ two hardware platforms from Decawave: DWM1001-dev and EVK1000. They use different peripherals, antennas, clocks, and on-board controllers, but do utilize the same

DW1000 transceiver [7]. This transceiver complies with the IEEE 802.15.4-2011 standard and allows bandwidths of up to 1300 MHz. For regulatory constraints, we allocate a 500 MHz bandwidth at a carrier frequency of 4.3 GHz. Although larger bandwidths are theoretically more advantageous for timestamping in multipath environments, we found that the distance measurements remain the same at different bandwidths in our setup with our technique. This is, at least partly, due to small payloads comprising of two 64-bit timestamps and two 32-bit IDs. The use of such short messages helps to obtain accurate timestamps and thus improves ranging.

2.2 Network Architecture

A node discovery scheme enables devices to seamlessly join the network. As devices leave or appear non-responsive (e.g., due to an empty battery or being out-of-range), a scheduler marks these devices and removes them if they miss update requests. A load balancing protocol distributed resources among devices. A dynamic time division multiple access (TDMA) scheme is used to allocate time slots to devices. Contention-free medium access allows for deterministic transmissions without inter-symbol-interference and a high degree of duty-cycling. A dedicated slot is reserved for the load balancing to disseminate system-relevant information, such as re-allocation of slots to devices. The schedulers are operated by a lead-AP determined by auctioning. In case of a non-responsive lead-AP, its successor takes over after a timeout. To optimize the execution time and coverage, a cell-based approach is adopted to assign devices to their nearest lead-AP. Within a cell, the results for distance measurements are embedded into the ranging protocol to disseminate distance information without the need for dedicated messages.

2.3 Experimental Setup and Testbeds

Two static environments serve as testbeds to showcase the capabilities of HiPR+ for ranging and localization. For consistent and fair comparison, all tests are replicated on both hardware platforms with HiPR+ and Decawave's native solution.

Both testbeds are operated with a single tag. The first testbed (Fig. 1a) consists of a single AP that performs continuous distance measurements to the tag. Whereas the AP remains at its fixed location, the tag is positioned at eight different locations, ranging from 50 cm to 400 cm away from the AP. The second testbed (Fig. 1b) consists of six APs, where five are at similar heights (2 m) and the sixth is deployed at the ceiling (4 m). This setup is used to evaluate the effects of different APs constellations and to assess the performance of three different localization techniques.

The ground truth is established using a laser ranger with an accuracy of ± 2 mm (Bosch PLR 50 C). To counterbalance inaccuracies due to deep notches on the antennas vertical axis, the devices are faced toward each other. All tests are performed under identical conditions with more than 1000 measurements at each test location to ensure a certain level of statistical confidence.

3 RANGING

The goal of ranging is to estimate the physical distance between two devices. We propose here a ranging technique (as part of HiPR+) that is based on the ranging technique HiPR [23] but extends and

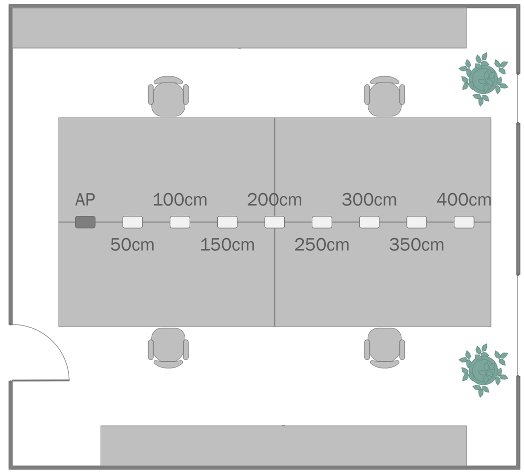

(a) One access point and a single tag deployed at eight test positions between 50 cm and 400 cm.

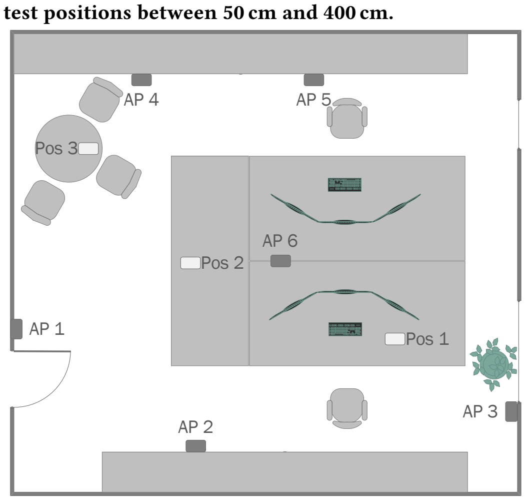

(b) Six access points and a single tag deployed at three test positions.

Figure 1: Static test environments

improves it. The main modifications are: reduction of the network load with continuous estimates, antenna delay calibration, and distance compensation. Furthermore, the new approach is tested on two different hardware platforms. The definitions and concepts are explained in the following. All definitions and some concepts are the same as in HiPR [23]; nevertheless, they are repeated here for completeness and self-consistency of the paper at hand.

3.1 Accuracy and Precision

Two devices located at distance d from each other perform multiple distance measurements between each other. Each measurement $i \in \mathbb{N}$ yields a distance estimate $\hat{d}_i$, which suffers from an estimation *error* $\epsilon_i(d) = \hat{d}_i - d$. We only require the absolute error $|\epsilon_i(d)|$.

Ideally, a ranging technique is accurate and precise. It is accurate if the average distance estimate is close to the actual distance. The *accuracy* is the average value of the distance errors, i.e., $\bar{\epsilon}(d) = \frac{1}{n}\sum_{i=1}^{n}\epsilon_i(d)$ with a sufficiently high number of estimates n. A ranging technique is precise if the distance estimates are close to each other. The *precision* is the variance of the errors, i.e., $\sigma_\epsilon^2(d) = \frac{1}{n-1}\sum_{i=1}^{n}(\epsilon_i(d) - \bar{\epsilon}(d))^2$.

3.2 Error Sources

The distance between two devices A and B is estimated based on the propagation time of a signal over the air between the devices. This time is often referred to as time of flight (ToF). The ranging used in this paper utilizes ToF and records the timestamps at which a message is transmitted or received. The simple difference between these two timestamps, denoted as propagation time T_{prop}, is, however, in general *not* a highly accurate ToF estimation, the reason being clock biases, clock drifts, inaccurate synchronization, and deficiencies in the timestamping process.

Transceivers can run slightly faster or slower than their nominal clock frequency f. Both of the hardware platforms used facilitate crystal oscillators with 20 ppm, which therefore imply inaccuracies of up to 20 μs. Assuming that each clock runs at factor k of the nominal clock frequency, i.e., $0.999980 \leq k \leq 1.000020$, the clock-induced error on the distance estimations can be described as [7]

$$T_{\text{ClkErr}} = T_{\text{prop}}\left(1 - \frac{k_A + k_B}{2}\right), \tag{1}$$

which yields inaccuracies of a few picoseconds only [7]. For a distance of $d = 100$ m, the clock-induced error results in a 6.7 ps inaccuracy, which relates to a distance error of 2.2 mm.

The delay between the timestamping process (e.g., triggering and acquisition) and the physical transmission or reception of a signal is assumed to be constant over time but in general different for each device. Such hardware-dependent offset is referred to as antenna delay and needs to be compensated. We calibrate all devices to a reference distance in order to ensure homogeneous distance acquisitions.

Small additional errors are caused by temperature and hardware-dependent tolerances and imprecise clocks with deviating offsets and drifts. These errors affect the ToF and accumulate over the measurement distances. Propagation models are applied to describe and compensate these errors.

3.3 Technique

HiPR+ builds upon the double-sided two-way ranging (DS-TWR) protocol [8, 14, 31] without device synchronization. A single pairwise distance measurement between two devices is shown in Fig. 2.

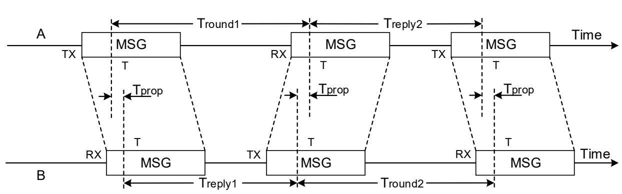

Figure 2: Double-sided two-way ranging protocol.

The symbol T marks the timestamps for transmission (TX) and reception (RX) with their propagation times T_{prop}. The durations for transmission or reception acknowledgments are T_{round} and T_{reply}. For each measurement i, the ToF is estimated by [6]:

$$\widehat{\text{ToF}} = \frac{T_{\text{round1}}\,T_{\text{round2}} - T_{\text{reply1}}\,T_{\text{reply2}}}{T_{\text{round1}} + T_{\text{round2}} + T_{\text{reply1}} + T_{\text{reply2}}}\,. \tag{2}$$

The timestamping process influences the ranging precision. We denote $T_{\text{TX}_{\text{real}}}$ and $T_{\text{RX}_{\text{real}}}$ as the real transmit and reception instants and compute for a generated timestamp T the values $T_{\text{TX}_{\text{real}}} = T + T_{\text{a}} + T_{\text{h}}$ for the transmission and $T_{\text{RX}_{\text{real}}} = T - T_{\text{a}}$ for the reception. The systematic antenna delay T_{a} occurs between the timestamp generation T and the moment a message is physically emitted or received; the processing delay T_{h} is the time required to add the timestamp T to the header of a message at the transmitter.

In contrast to the original DS-TWR protocol, HiPR+ utilizes hardware interrupts to trigger timestamps more accurately [23], i.e., as close as possible to $T_{\text{TX}_{\text{real}}}$ and $T_{\text{RX}_{\text{real}}}$. These timestamps are generated at time instants narrowly close to $T_{\text{TX}_{\text{real}}}$, this means that they cannot be embedded into the header of the message being transmitted at that time. Instead, HiPR+ includes the generated timestamps into the payload of the next message of the ranging

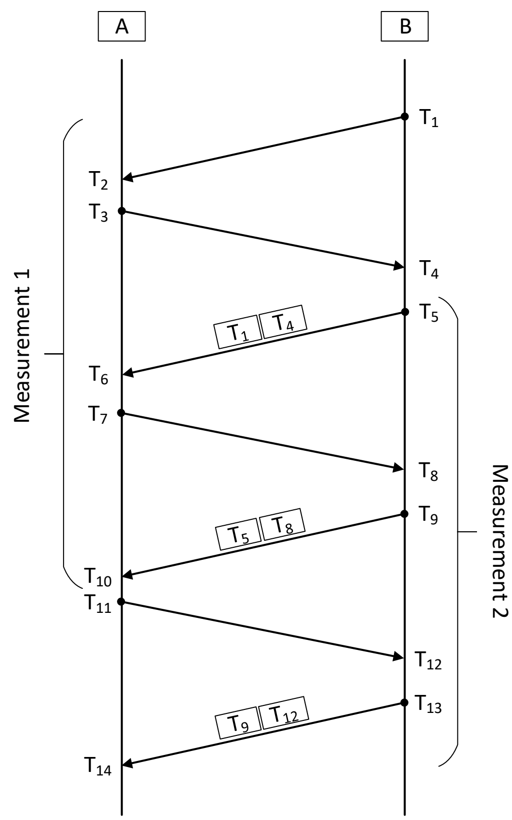

Figure 3: HiPR+ ranging utilizes continues measurements to reduce network load and optimize the execution time.

protocol. Therefore, this approach eliminates the processing delay T_h, for the cost of one additional message at the end of the ranging protocol to exchange all the timestamps.

In order to compensate the time for this additional signaling message and to reduce the overall network load, HiPR+ employs a concept for continuous operation. Multiple subsequent distance measurements are performed to improve the overall accuracy by averaging single distance estimates. Fig. 3 illustrates the procedures to maximize the number of range estimates while minimizing the number of exchanged messages. HiPR+ utilizes the last message of a measurement (third message in Fig. 2) as the first message of a subsequent measurement. This reduces the network load from $MSGs = 4n$ for n single measurements to $MSGs = (2n) + 2$. This reduces the processing and computation costs and yields faster distance acquisitions. HiPR+ also employs a generic strategy to minimize delays caused by frequent switching between transmission modes, e.g., transmission $\leftrightarrows$ reception. To obtain a number of n distance measurements, each message is re-transmitted n times in its respective direction. This reduces the switching effort from $2n$ for the DS-TWR to only 2. Furthermore, HiPR+ incorporates error handling procedures to detect and re-initiate messages efficiently. This reduces the messaging effort for a repeated measurement from $MSGs = 3$ for the DS-TWR to $MSGs = 1$.

3.4 Antenna Delay Compensation

To account for hardware-dependent antenna delays, each device is normalized with help of two other devices. The three devices are operated in a controlled environment, namely in an equilateral triangular setting with known lateral distance. Pairwise distance measurements are performed, yielding three estimations $\widehat{\text{ToF}}$ and three transceiver delays τ_i with device index $i \in \{A, B, C\}$. The overall transceiver delay comprises a transmission delay $\tau_i(\text{TX})$ and a reception delay $\tau_i(\text{RX})$, where $\tau_i = \tau_i(\text{TX}) + \tau_i(\text{RX})$. These delays are shown in Fig. 4. In general, $\tau_i(\text{TX})$ is different to $\tau_i(\text{RX})$, which requires a rearrangement of the triangular order to attain fully-meshed distance measurements. However, the resulting inaccuracy is marginal and a rearrangement induces slight variations in the deployment, which affects the ground truths, antenna radiation patterns, and the multipath propagation. We therefore assume that $\tau_i(\text{TX})$ and $\tau_i(\text{RX})$ are identical for each device i, but τ_i is different on every device.

One thousand pairwise measurements are performed, yielding two round and two reply durations for each measurement (Fig. 2 and (2)). With the known lateral distance of the equilateral triangle, the pairwise ToF can be estimated by

$$\widehat{\text{ToF}}_{ij} = \frac{(T_\text{round1} - \tau_i)(T_\text{round2} - \tau_j)}{T_\text{round1} + T_\text{round2} + T_\text{reply1} + T_\text{reply2}} - \frac{(T_\text{reply1} + \tau_j)(T_\text{reply2} + \tau_i)}{T_\text{round1} + T_\text{round2} + T_\text{reply1} + T_\text{reply2}}$$

with two devices $i, j \in \{A, B, C\}$ with $i \neq j$.

The hardware-specific antenna delays are stored on each device individually. This allows the devices to exchange their values during the ranging procedure. As a result, the antenna delays of both devices can be considered in the ToF estimation — performed on each device — to attain a higher precision and accuracy.

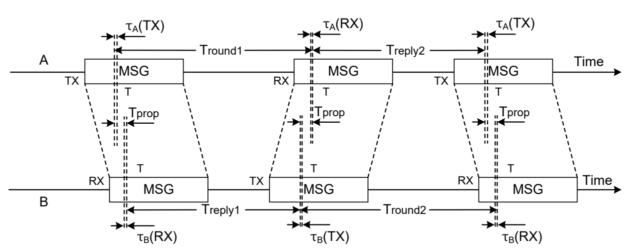

Figure 4: HiPR+ ranging protocol with interrupt driven timestamping and antenna delays.

3.5 Experimental Evaluation

We now evaluate the precision and accuracy of the HiPR+ ranging protocol on two hardware platforms and compare the results to Decawave's native solution. Hardware calibration methods are discussed and evaluated in the test environment 1a.

Precision and Accuracy. Fig. 5 summarizes the results of distance measurements at eight test locations ranging from 50 cm to 400 cm. Fig. 5(a) shows the performance of Decawave's native technique as baseline. Figs. 5(b) and (c) show HiPR+ with its extended DS-TWR protocol, precise timestamping, error handling, and antenna delay compensation for two different hardware platforms. The native technique has an average variance (precision) of more than 5 cm with inaccuracies from 19 cm to 37 cm. HiPR+ achieves an average precision of 0.15 cm with inaccuracies from 5 cm to 20 cm. HiPR+ on the DWM1000C platform has the fewest outliers and the highest linearity of inaccuracies accumulation over increasing distance.

Antenna Delay Compensation. The antenna delay compensation, as described in Section 3.4, ensures that the devices are normalized to a known reference distance. This ensures identical behavior and unified distance estimation of all devices at this reference distance. However, a perfect compensation is not attainable, given that errors are multiplied with the speed-of-light for each estimation. It can thus be assumed that minor inaccuracies remain on each hardware, which affect the distance estimation over larger ToF durations. The increase however is consistent for all devices and can thus be modeled and compensated. In contrast to the native technique, HiPR+ is able to use a computationally inexpensive first degree polynomial to account for these errors. The low complexity of the model allows for its integration on the hardware to correct ToF estimations. No edge computation or server infrastructure is required for post-processing of distance estimations. Fig. 6 shows the results of the distance measurements with inaccuracy compensation, evaluated in testbed 1a. Whereas the native technique has an average inaccuracy of −1.3 cm, HiPR+ reduces this error to 0.7 cm and 0.5 cm for the EVK1000 and DWM1000C platform, respectively. The ground truth is obtained at the 100 cm test location, as a result to the antenna delay compensation at this distance.

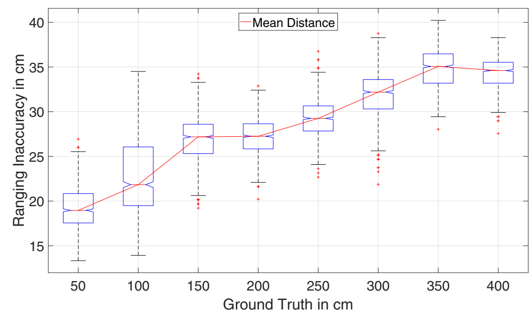

(a) Decawave's native solution on the EVK1000 platform.

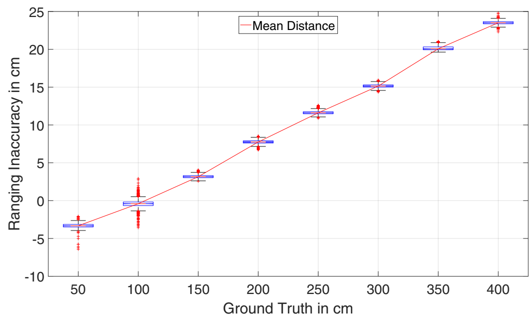

(b) HiPR+ ranging on the EVK1000 platform.

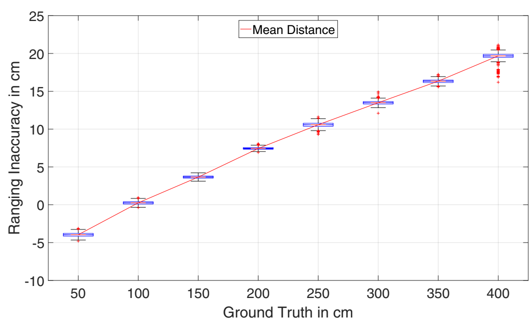

(c) HiPR+ ranging on the DWM1000C platform.

Figure 5: Accuracy and precision of different ranging techniques (without distance compensation) on different hardware platforms in testbed 1a.

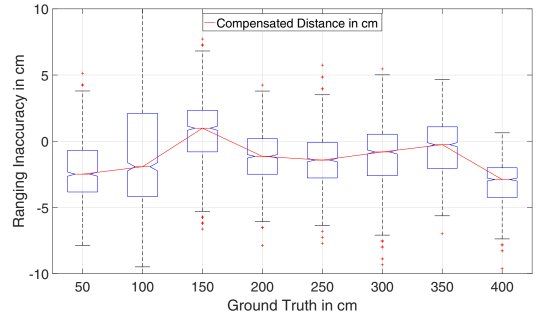

(a) Decawave's native solution on the EVK1000 platform.

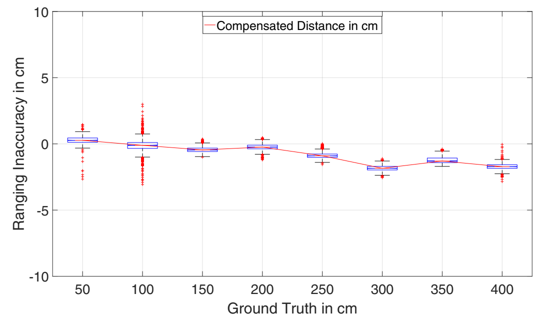

(b) HiPR+ ranging on the EVK1000 platform.

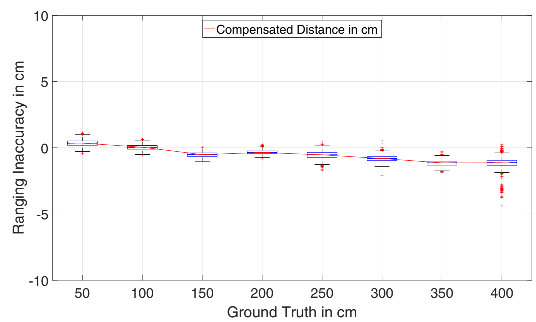

(c) HiPR+ ranging on the DWM1000C platform.

Figure 6: Accuracy and precision of different ranging techniques (with compensation) on different hardware platforms in testbed 1a.

4 POSITIONING

We now apply different localization techniques on top of the distance estimation: a time-of-arrival technique, a least square error technique, and an extended Kalman filter. The 3D accuracy is evaluated in testbed 1b.

4.1 Techniques

For a tag located at position $\mathbf{p} = (x, y, z)^T$, the goal of localization is to determine a good estimate $\hat{\mathbf{p}} = (\hat{x}, \hat{y}, \hat{z})^T$. This is done with help of multiple APs (indexed by $i \in \mathbb{N}$) at known positions $\mathbf{p}_i = (x_i, y_i, z_i)^T$. Distance measurements are made from the tag to each AP, where the estimated distance between tag and AP i is denoted by $\hat{d}_i$. The tag velocity is $\mathbf{v} = (v_x, v_y, v_z)^T$.

4.1.1 Baseline. A time-of-arrival-based multi-lateration localization, described in [27], serves as a baseline approach (BLA). Without loss of generality we assume that the origin is located at AP1, i.e., $\mathbf{p}_1 = \mathbf{0}$. The locations of all other APs are written in a matrix

$$\mathbf{H} = \begin{bmatrix} \mathbf{p}_2^T \\ \mathbf{p}_3^T \\ \mathbf{p}_4^T \\ \vdots \end{bmatrix} = \begin{bmatrix} x_2 & y_2 & z_2 \\ x_3 & y_3 & z_3 \\ x_4 & y_4 & z_4 \\ \vdots & \vdots & \vdots \end{bmatrix}. \tag{3}$$

The tag position can be estimated by $\hat{\mathbf{p}} = (\mathbf{H}^T\mathbf{H})^{-1}\mathbf{H}^T\mathbf{b}$ [27] with

$$\mathbf{b} = \frac{1}{2}\begin{bmatrix} \|\mathbf{p}_2\|^2 - |\hat{d}_2^2 - \hat{d}_1^2| \\ \|\mathbf{p}_3\|^2 - |\hat{d}_3^2 - \hat{d}_1^2| \\ \|\mathbf{p}_4\|^2 - |\hat{d}_4^2 - \hat{d}_1^2| \\ \vdots \end{bmatrix}. \quad (4)$$

4.1.2 Least Squared Error. Given the estimated distances, the least squared error (LS) technique computes the tag position that minimizes the sum of the squared errors between the real and estimated distances:

$$\hat{\mathbf{p}} = \underset{x,y,z}{\operatorname{argmin}} \sum_i \left(\|\mathbf{p}_i - \mathbf{p}\| - \hat{d}_i\right)^2. \quad (5)$$

Such optimization problem can be solved by an iterative procedure or by linearization. We employ the iterative Newton Raphson algorithm, which is a non-linear LS approach with a higher computational complexity but better accuracy than a linear LS algorithm.

4.1.3 Extended Kalman Filter (EKF). We define the state vector to be estimated by the EKF as $\mathbf{x} = (x, v_x; y, v_y; z, v_z)^T$. The positioning problem is a discrete-time process with a state model $\mathbf{x}_k = f(\mathbf{x}_{k-1}) + \mathbf{w}_{k-1}$ and a measurement model $\mathbf{z}_k = g(\mathbf{x}_k) + \mathbf{v}_k$ (k refers to the discrete-time instant). The function $f(\mathbf{x})$ models the kinematic movement of a tag; the other function is $g(\mathbf{x}) = \|\mathbf{p} - \mathbf{p}_i\|$. The usage of the EKF rather than the Kalman filter results from the non-linearity of these measurement equations. The terms $\mathbf{w}_k \sim \mathcal{N}(\mathbf{0}, \mathbf{Q}_k)$ and $\mathbf{v}_k \sim \mathcal{N}(\mathbf{0}, \mathbf{R}_k)$ represent the process noise and measurement noise with autocovariance matrices $\mathbf{Q}$ and $\mathbf{R}$. We set $\mathbf{R}$ as the diagonal matrix where the diagonal elements correspond to the variances of estimated ranges σ_i^2 between the receiver and AP$_i$. The noise autocovariance matrix is then formulated as follows: $\mathbf{R} = \operatorname{diag}(\sigma_i^2)_{1 \le i \le N}$. σ_i is computed using a moving average over the variance and initiated with the value 0.81 cm from Section 3. $\mathbf{Q}$ accounts for the kinematic movement equations.

4.2 Experimental Evaluation

The three localization techniques are evaluated in testbed 2 (Fig. 1b) for two AP constellations with and without antenna delay calibration, marked as *calibrated* (cal.) and *uncalibrated* (uncal.). The effects of distance inaccuracy *compensation* (comp.) are also given.

Table 1: Errors of 3D positioning techniques.

	Median 3D positioning error in cm		
	EKF	LS	BLA
5 APs cal.	41.7	225.3	634
5 APs cal. comp.	20.2	168.8	326.1
6 APs uncal.	27.5	136	59.6
6 APs uncal. comp.	7.8	146.2	7.8
6 APs cal.	16	142	52.2
6 APs cal. comp.	0.8	155.7	3.6

The results show that the AP constellation is a key factor in obtaining sub-centimeter localization. A circular deployment achieves accurate estimations in the x-y-plane but not in the height (z). It yields the largest 3D errors for all evaluated techniques, with the BLA being particularly inaccurate (see Fig. 7(a)). The use of an additional AP at the ceiling of the room substantially helps to achieve a more precise height estimation. The results in Figs. 7(b) and (c) show improved 3D accuracies for all three techniques with the BLA outperforming the LS approach. The use of inaccuracy compensation appears decremental for the LS whereas it improves the BLA and EKF to 3.6 cm and 0.8 cm, respectively as illustrated in Table 1. The

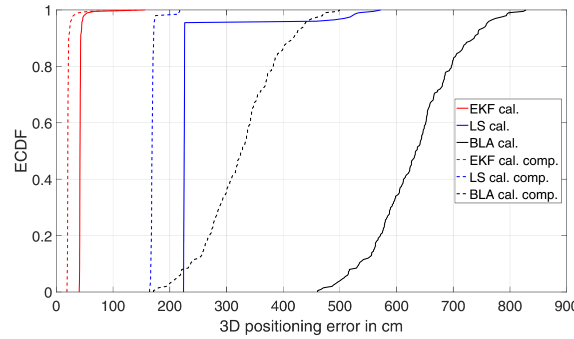

(a) DWM1000C platform, APs 1-5.

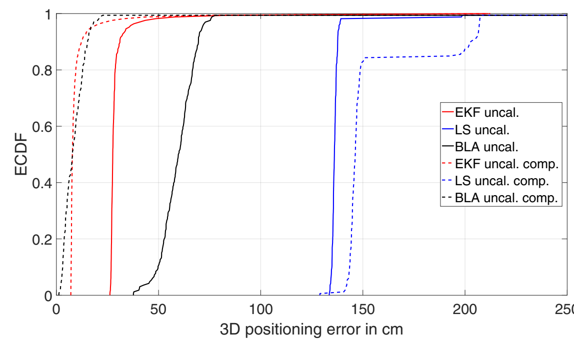

(b) DWM1000C platform, 6APs uncalibrated.

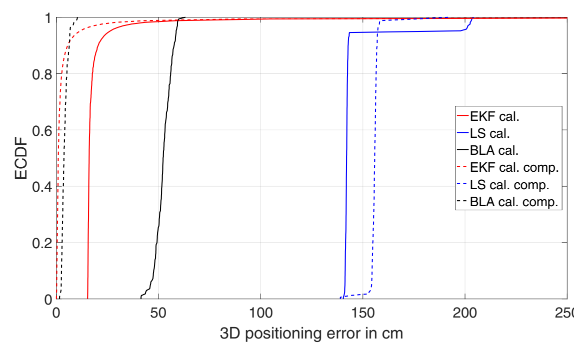

(c) DWM1000C platform, 6APs calibrated.

Figure 7: Empirical cumulative distribution function of the 3D positioning error for three localization techniques, two AP constellations, with/without antenna delay calibration (cal./uncal.) and inaccuracy compensation (comp.).

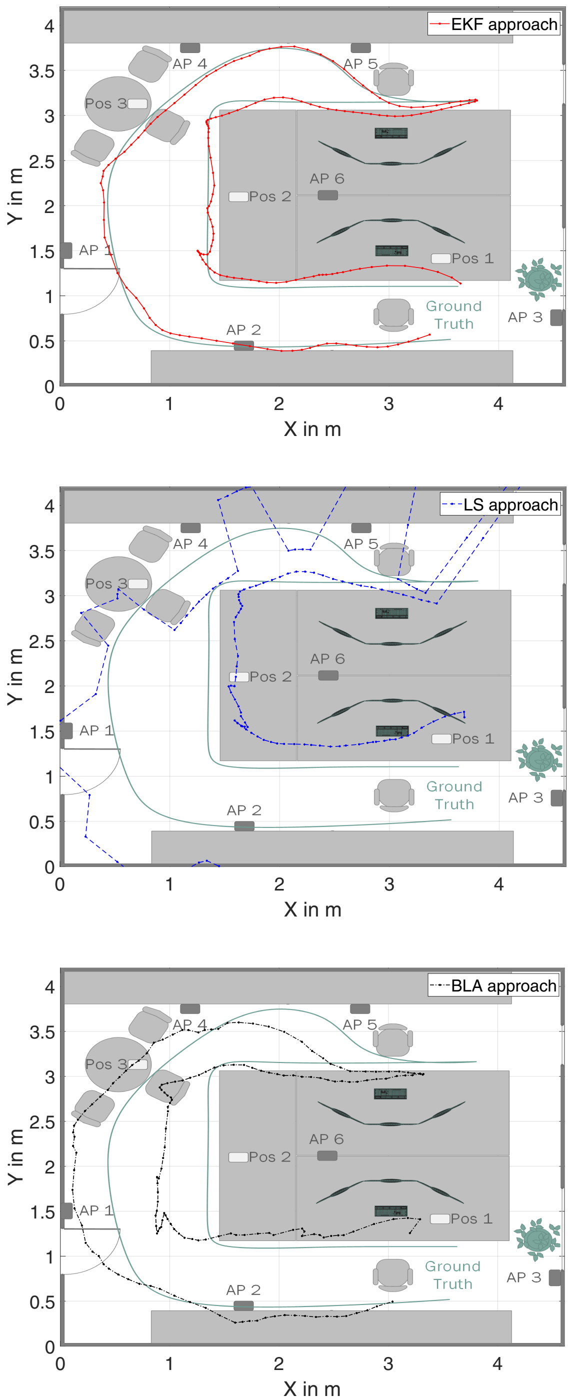

(c) BLA approach.

Figure 8: Visualization of the tracking result for a tag operated in an office environment with six APs.The ground truth of the movement path is marked and the tag velocity and height can be assumed to be constant.

best overall accuracy can be obtained with the EKF. These results are consistent with the experimental findings in [9] of LS and EKF for ToF localization with Wi-Fi and GPS. The measurements show that antenna delay calibration is the basis for quick convergence to accurate positions. Compensating the distance inaccuracies is essential to obtain sub-centimeter accuracy. This becomes even more essential in larger setups.

4.3 Tracking

In addition to the localization of *static* tags done above, we evaluate the performance in a *mobile* setup (tracking). Tags move on a predefined path through an office with a constant velocity at a constant height. Fig. 8 illustrates the 2D trajectory as estimated by the localization techniques (red, blue, or black traces) and compare it to the ground truth (green lines).

As expected, the EKF tracks the movement path with the highest accuracy. It captures both the target mobility thanks to its kinematic motion-based prediction and the noise affecting the ranging measurements. The LS seems to track the path moderately well when moving on a straight line but shows high deviations for circular motion. This behavior does not improve by applying weights to the LS. The BLA, despite being the fastest approach tested, shows the largest inaccuracy and struggles to track the tag.
Overall, the EKF demonstrates the best tracking performance, and we believe that it can further improve with additional IMU sensor fusion at the correction phase.

5 RELATED WORK

Localization systems are distinguished based on their technology [5, 22] and technique [4]. Commonly-used techniques exploit radio signal strength (RSS), time of arrival (ToA), time difference of arrival (TDoA), angle of arrival (AoA), and hybrid forms [10, 11, 13, 18, 20, 24, 30, 34]. Indoor localization is an emerging field with various applications [1, 15, 16]. A comparison of different technologies [35] indicates that UWB is a potential candidate with accurate ranging, moderate power consumption, and interference mitigation [2]. We build upon related work [3, 19] and use an asymmetric ToA two-way-ranging approach [8, 14, 31]. The calibration, clock drift correction, and time-of-flight error is addressed in recent publications [26, 28, 33]. A performance comparison of three commercially available UWB platforms (Decawave, BeSpoon and Ubisense) in indoor and outdoor experiments were conducted [17, 25]. The results indicate that Decawave performs best due to its advanced antenna system [12, 21]. Two studies on precise UWB localization [29, 32] show variances around 5 cm, which is in line with our own results with Decawave's native solution.

6 CONCLUSIONS AND OUTLOOK

HiPR+ is an experimentally tested UWB-based approach for centimeter-accurate indoor localization. Its functionality includes two layers: ranging and positioning. The ranging part is an improved version of HiPR [23], which is multiple times faster and more precise than Decawave's native solution. Integral parts are compensations of antenna delay and distance inaccuracy. The positioning part uses EKF on top of the ranging. Sub-centimeter 3D localization and tracking can be achieved in a laboratory setup. Future extensions can include IMU sensor fusion, a mapping service, and more optimized kinematic models for the EKF.

REFERENCES

[1] Klaithem Al Nuaimi and Hesham Kamel. 2011. A survey of indoor positioning systems and algorithms. In *Proc. IEEE Int. Conf. on Innovations in Information Technology (IIT)*. 185–190.

[2] Abdulrahman Alarifi, AbdulMalik Al-Salman, Mansour Alsaleh, Ahmad Alnafessah, Suheer Al-Hadhrami, Mai Al-Ammar, and Hend Al-Khalifa. 2016. Ultra wideband indoor positioning technologies: Analysis and recent advances. *Sensors* 16, 5 (2016), 707.

[3] K. Balac, M. Akhmedov, M. Prevostini, and M. Malek. 2016. Topology Optimization of Wireless Localization Networks. In *Proc. Int. Conf. European Wireless*.

[4] Juan Chóliz, Miguel Eguizabal, Ángela Hernández-Solana, and Antonio Valdovinos. 2011. Comparison of algorithms for UWB indoor location and tracking systems. In *Proc. IEEE Int. Conf. on Vehicular Technology Conference (VTC)*. 1–5.

[5] Jussi Collin, Oleg Mezentsev, Gérard Lachapelle, et al. 2003. Indoor positioning system using accelerometry and high accuracy heading sensors. In *Proc. ION GPS/GNSS Conf.* 9–12.

[6] DecaWave. 2015. *APS013 Application Note: The Implementation of Two-way Ranging with the DW1000, Version 2.2.* Technical Report.

[7] DecaWave. 2015. *DW1000 User Manual: How to Use, Configure and Program the DW1000 UWB Transceiver, Version 2.05.* Technical Report.

[8] Anday Duru, Eftal Şehirli, and İdris Kabalcı. 2018. Ultra-Wideband Positioning System Using TWR and Lateration Methods. In *Proc. ACM Int. Conf. Eng. & MIS*. 58.

[9] Aymen Fakhreddine, Domenico Giustiniano, and Vincent Lenders. 2016. Evaluation of self-positioning algorithms for time-of-flight based localization. In *2016 14th International Symposium on Modeling and Optimization in Mobile, Ad Hoc, and Wireless Networks (WiOpt)*. IEEE, 1–8.

[10] Aymen Fakhreddine, Domenico Giustiniano, and Vincent Lenders. 2018. Data fusion for hybrid and autonomous time-of-flight positioning. In *2018 17th ACM/IEEE International Conference on Information Processing in Sensor Networks (IPSN)*. IEEE, 266–271.

[11] Waldemar Gerok, Jürgen Peissig, and Thomas Kaiser. 2012. TDOA assisted RSSD localization in UWB. In *Proc. IEEE Workshop on Positioning, Navigation and Communication*. 196–200.

[12] Frank Hartmann, Christian Enders, and Wilhelm Stork. 2016. Ranging errors in UWB networks and their detectability. In *Proc. IEEE Int. Conf. on Telecommunications and Signal Processing (TSP)*. 194–198.

[13] Mark Hedley and Qiwei Zhai. 2014. Wireless sensor network using hybrid TDOA/RSS tracking of uncooperative targets. In *Proc. IEEE Int. Symp. on Wireless Personal Multimedia Communications (WPMC)*. 385–390.

[14] Kristóf Attila Horváth, Gergely Ill, and Ákos Milánkovich. 2017. Passive extended double-sided two-way ranging algorithm for UWB positioning. In *Proc. IEEE Int. Conf. on Ubiquitous and Future Networks (ICUFN)*. IEEE, 482–487.

[15] Faheem Ijaz, Hee Kwon Yang, Arbab Waheed Ahmad, and Chankil Lee. 2013. Indoor positioning: A review of indoor ultrasonic positioning systems. In *Proc. IEEE Int. Conf. on Advanced Communications Technology (ICACT)*. 1146–1150.

[16] Gints Jekabsons, Vadim Kairish, and Vadim Zuravlyov. 2011. An analysis of Wi-Fi based indoor positioning accuracy. *Scientific Journal of Riga Technical University* 44, 1 (2011), 131–137.

[17] Antonio Ramón Jiménez and Fernando Seco. 2016. Comparing Decawave and Bespoon UWB location systems: Indoor/outdoor performance analysis. In *Proc. IEEE Int. Conf. on Indoor Positioning and Indoor Navigation (IPIN)*. 1–8.

[18] Joon-Yong Lee and R. A. Scholtz. 2002. Ranging in a dense multipath environment using an UWB radio link. *IEEE Journal on Selected Areas in Communications* 20, 9 (Dec 2002), 1677–1683. https://doi.org/10.1109/JSAC.2002.805060

[19] Juraj Ko et al. 2016. Target tracking algorithms for UWB radar network. In *Proc. IEEE Int. Conf. Radioelektronika*. 319–324.

[20] David Macii, Alessio Colombo, Paolo Pivato, and Daniele Fontanelli. 2013. A data fusion technique for wireless ranging performance improvement. *IEEE Trans. Instrumentation and Measurement* 62, 1 (2013), 27–37.

[21] Marko Malajner, Peter Planinšič, and Dušan Gleich. 2015. UWB ranging accuracy. In *Proc. IEEE Int. Conf. on Systems, Signals and Image Processing (IWSSIP)*. 61–64.

[22] Rainer Mautz. 2012. *Indoor positioning technologies.* Technical Report. ETH Zurich, Department of Civil, Environmental and Geomatic Engineering.

[23] D. Neuhold, C. Bettstetter, and A. F. Molisch. 2019. HiPR: High-Precision UWB Ranging for Sensor Networks. In *Proc. ACM Intern. Conf. on Modeling, Analysis and Simulation of Wireless and Mobile Systems (MSWiM)*. Miami Beach, FL, USA, 103–107. https://doi.org/10.1145/3345768.3355931

[24] Luis Oliveira, Carmelo Di Franco, Traian E Abrudan, and Luis Almeida. 2013. Fusing time-of-flight and received signal strength for adaptive radio-frequency ranging. In *Proc. IEEE Int. Conf. on Advanced Robotics (ICAR)*. 1–6.

[25] Antonio Ramón Jiménez Ruiz and Fernando Seco Granja. 2017. Comparing ubisense, bespoon, and decawave uwb location systems: Indoor performance analysis. *IEEE Trans. Instrumentation and Measurement* 66, 8 (2017), 2106–2117.

[26] Cung Lian Sang, Michael Adams, Timm Hörmann, Marc Hesse, Mario Porrmann, and Ulrich Rückert. 2018. An Analytical Study of Time of Flight Error Estimation in Two-Way Ranging Methods. In *Proc. IEEE Int. Conf. Indoor Pos. and Indoor Navigation (IPIN)*. 1–8.

[27] Ali H Sayed, Alireza Tarighat, and Nima Khajehnouri. 2005. Network-based wireless location: challenges faced in developing techniques for accurate wireless location information. *IEEE Signal Processing Mag.* 22, 4 (2005), 24–40.

[28] Juri Sidorenkoab, Volker Schatza, Norbert Scherer-Negenborna, Michael Arensa, and Urs Hugentobler. 2019. Decawave UWB clock drift correction and powerself-calibration. *ArXiv preprint: 1902.11085* (2019).

[29] Bruno Silva, Zhibo Pang, Johan Åkerberg, Jonas Neander, and Gerhard Hancke. 2014. Experimental study of UWB-based high precision localization for industrial applications. In *Proc. IEEE Int. Conf. on Ultra-WideBand (ICUWB)*. 280–285.

[30] Zhenlong Song, Gangyi Jiang, and Chao Huang. 2011. A survey on indoor positioning technologies. In *Proc. Int. Conf. on Theoretical and Mathematical Foundations of Computer Science*. Springer, 198–206.

[31] Simon Tewes, Ludwig Schwoerer, and Patrick Bosselmann. 2017. Designing a Basic IR-UWB-RTLS-Raw-data position estimation utilizing TWR. In *Proc. Int. Conf. on European Conference on Smart Objects, Systems and Technologies (Smart SysTech)*.

[32] Jia Wang, Asad Khalid Raja, and Zhibo Pang. 2015. Prototyping and experimental comparison of IR-UWB based high precision localization technologies. In *Proc. IEEE Int. Conf. on on Ubiquitous Intelligence and Computing and IEEE Int. Conf. on Autonomic and Trusted Computing and Proc. IEEE Int. Conf. on Scalable Computing and Communications and Its Associated Workshops (UIC-ATC-ScalCom)*. 1187–1192.

[33] Gui Xinzhe, Shuli Guo, Qiming Chen, and Lina Han. 2018. A New Calibration Method of UWB Antenna Delay Based on the ADS-TWR. In *Proc. IEEE Chinese Control Conference (CCC)*.

[34] Ali Yassin, Youssef Nasser, Mariette Awad, Ahmed Al-Dubai, Ran Liu, Chau Yuen, Ronald Raulefs, and Elias Aboutanios. 2016. Recent advances in indoor localization: A survey on theoretical approaches and applications. *IEEE Communications Surveys & Tutorials* 19, 2 (2016), 1327–1346.

[35] Faheem Zafari, Athanasios Gkelias, and Kin K Leung. 2019. A survey of indoor localization systems and technologies. *IEEE Communications Surveys & Tutorials* 1 (2019).